Synergy of Radiotherapy and a Cancer Vaccine for the Treatment of HPV-Associated Head and Neck Cancer

Michele Mondini[1], Mevyn Nizard[2], Thi Tran[2], Laetitia Mauge[2,3], Mauro Loi[1,4], Céline Clémenson[1], Delphine Dugue[1], Pierre Maroun[1,5,6], Emilie Louvet[7,8], Julien Adam[7,8], Cécile Badoual[2,9], Dominique Helley[2,3], Estelle Dransart[10], Ludger Johannes[10], Marie-Catherine Vozenin[1,6,11], Jean-Luc Perfettini[1,6,8], Eric Tartour[2,12], and Eric Deutsch[1,5,6,8]

Abstract

There is growing interest in the association of radiotherapy and immunotherapy for the treatment of solid tumors. Here, we report an extremely effective combination of local irradiation (IR) and Shiga Toxin B (STxB)–based human papillomavirus (HPV) vaccination for the treatment of HPV-associated head and neck squamous cell carcinoma (HNSCC). The efficacy of the irradiation and vaccine association was tested using a model of HNSCC obtained by grafting TC-1/luciferase cells at a submucosal site of the inner lip of immunocompetent mice. Irradiation and the STxB-E7 vaccine acted synergistically with both single and fractionated irradiation schemes, resulting in complete tumor clearance in the majority of the treated mice. A dose threshold of 7.5 Gy was required to elicit the dramatic antitumor response. The combined treatment induced high levels of tumor-infiltrat-

ing, antigen-specific CD8$^+$ T cells, which were required to trigger the antitumor activity. Treatment with STxB-E7 and irradiation induced CD8$^+$ T-cell memory, which was sufficient to exert complete antitumor responses in both local recurrences and distant metastases. We also report for the first time that a combination therapy based on local irradiation and vaccination induces an increased pericyte coverage (as shown by αSMA and NG2 staining) and ICAM-1 expression on vessels. This was associated with enhanced intratumor vascular permeability that correlated with the antitumor response, suggesting that the combination therapy could also act through an increased accessibility for immune cells. The combination strategy proposed here offers a promising approach that could potentially be transferred into early-phase clinical trials. *Mol Cancer Ther; 14(6); 1336–45. ©2015 AACR.*

Introduction

Human papillomavirus (HPV) is the most common sexually transmitted infection in Western countries (1, 2). Mucosal infec-

tion with "high-risk" HPV types (e.g., HPV16) has long been acknowledged to be a major risk factor for malignant neoplasms such as cervical, anal, penile, vaginal, and head and neck squamous cell carcinoma (HNSCC). The global burden of cancers attributable to HPV infection is estimated at 600,000 cases per year worldwide (3) and accounts for up to 40% to 90% of oropharyngeal cancers with a steadily increasing rate (4).

Research has demonstrated that HPV-related HNSCC represents a distinct subgroup of malignancies with improved outcomes compared with HPV-negative HNSCC; this is a result of a combination of peculiar biologic features and favorable patient characteristics (younger patients and a minor role for tobacco and alcohol abuse; refs. 5, 6). These patients are also more likely to have a durable benefit from radiotherapy, which is recognized as a valuable option for HNSCC (7). Because of the increasing incidence of HPV-related cancers and the promising results of radiotherapy, there is a need for the further optimization of radiotherapy treatments by integrating novel strategies to improve its therapeutic index and limit the dose-related toxicity.

Except in rare cases (8), cancer vaccines showed negative results as a standalone therapy (9). Nevertheless, they might have utility when used in combination with radiotherapeutic treatments (10, 11). Indeed, some of the effects of ionizing radiation are now recognized as contributing to antitumor immunity (12). It has been proposed that radiation-induced modifications of the microenvironment can benefit the antitumor immune activity triggered by vaccination through several mechanisms (13). First, radiotherapy may drive anticancer immunity toward tumor-related antigens and act as an adjuvant to boost antigen presentation

[1]INSERM U1030 «Radiothérapie Moléculaire», Gustave Roussy Cancer Campus Grand Paris, Villejuif, France and Labex LERMIT. [2]INSERM U970, PARCC (Paris Cardiovascular Research Center), Université Paris Descartes, Sorbonne Paris-Cité, Paris, France. [3]Service d'Hématologie Biologique, Hôpital Européen Georges-Pompidou, AP-HP, Paris, France. [4]Radioterapia, Università di Firenze, Florence, Italy. [5]Département de Radiothérapie, Gustave Roussy Cancer Campus Grand Paris, Villejuif, France. [6]Université Paris Sud, Faculté de Médecine du Kremlin-Bicêtre, France. [7]INSERM U981, Gustave Roussy Cancer Campus Grand Paris, Villejuif, France. [8]SIRIC SOCRATE, Villejuif Cedex, France. [9]Service d'Anatomie Pathologique, Hôpital Européen Georges-Pompidou, AP-HP, Paris, France. [10]Institut Curie, U1143 INSERM, UMR3666 CNRS, Endocytic Trafficking and Intracellular Delivery Group, Paris, France. [11]Laboratoire de Recherche en Radio-Oncologie, CHUV, Lausanne, Switzerland. [12]Service d'Immunologie Biologique, Hôpital Européen Georges-Pompidou, AP-HP, Paris, France.

Note: Supplementary data for this article are available at Molecular Cancer Therapeutics Online (http://mct.aacrjournals.org/).

M. Nizard, T. Tran, and L. Mauge contributed equally to this article.

Corresponding Author: Eric Deutsch, INSERM U1030 «Radiothérapie Moléculaire», Gustave Roussy Cancer Campus Grand Paris, 114 rue Edouard Vaillant, Villejuif 94805, France. Phone: 331-4211-6573; Fax: 331-4211-5236; E-mail: eric.deutsch@gustaveroussy.fr

doi: 10.1158/1535-7163.MCT-14-1015

©2015 American Association for Cancer Research.

AACR

(14, 15). In addition, radiotherapy could act as a vascular remodeling agent, promoting the recruitment of inflammatory cells and the infiltration of activated immune effectors to disrupt the tolerance related to an immunosuppressive tumor microenvironment (16).

The B subunit of the Shiga toxin (STxB) is a nonreplicative vector that targets dendritic cells (DC) *in vivo* (17). When coupled to various tumor antigens, it elicits a strong induction of specific CD8$^+$ T cells, which can be further enhanced by the addition of adjuvants (18). The STxB-based vaccine used in the present study (STxB-E7) carries an epitope from the HPV16 E7 oncoprotein, which is actively expressed in HPV-related HNSCC (19). We recently showed that mucosal (intranasal) immunization with STxB-E7 elicits a sustained antitumor response in a murine model of HPV-positive HNSCC (20). However, the therapeutic efficacy of the vaccine was limited when it was administered by a systemic route.

The purpose of our study was to test whether local irradiation could boost the efficacy of the novel STxB-E7 vaccine to treat HNSCC. We thereby used an immunocompetent mouse model of HPV-related HNSCC and, by different radiation schedules, demonstrated synergistic activity of the irradiation and vaccination. To elucidate the mechanisms underlying the interaction between STxB-E7 and radiotherapy, we focused our analysis on the tumor-infiltrating immune cells and the vascularization pattern. We showed that irradiation promoted HPV-E7–specific CD8$^+$ T-cell tumor infiltration and vascular normalization in vaccinated tumors, suggesting that the combination therapy acts both through increased levels and tumor accessibility of cytolytic CD8$^+$ T cells.

Materials and Methods

Cells

Firefly luciferase-expressing TC1/Luc cells, generated by the HPV16 E6/E7 and c-H-ras retroviral transduction of lung epithelial cells of C57BL/6 origin, were kindly provided by T.C. Wu (Johns Hopkins Medical Institutions, Baltimore, MD) in 2009. The cells were cultured *in vitro* in RPMI-1640 supplemented with 10% FBS, 1% sodium pyruvate, 1% non-essential amino acids, 10 mmol/L HEPES and 1% penicillin/streptomycin and were grown at 37°C with 5% CO$_2$. Master stocks of the cells were prepared upon receipt and then used within 6 months after resuscitation. Expression of E6 and E7 genes was confirmed by RT-PCR as previously described (21), as well as MHC haplotype H2^b by flow cytometry.

Head and neck tumor and lung metastasis models

Female C57BL/6 mice (age, 7 to 8 weeks) were purchased from Janvier CERT and housed in the Gustave Roussy animal facility. Animal procedures were performed according to the protocols approved by the Ethical Committee CEEA 26 and in accordance with recommendations for the proper use and care of laboratory animals. To establish a HNSCC implantation model, syngeneic tumor grafts were initiated at day 0 by injection of 0.1 mL of PBS suspension containing 5×10^5 TC1/Luc cells at a submucosal site of the right inner lip. For rechallenge experiments, mice were injected in the left inner lip. Lung metastases were established by injecting 10^6 TC1/Luc cells suspended in 0.2 mL of PBS in the tail vein. Throughout the study, the health, weight, and behavior of the mice was assessed

daily; mice were humanely euthanized upon the presentation of defined criteria (tumor size, ulceration, loss of >20% of the initial weight), and survival time was recorded to perform a survival analysis for the treatment groups.

Irradiation

Mice received single-beam local irradiation to the head and neck region using a 200 kV Varian X-ray irradiator. Selective irradiation of the tumor grafts was performed by the interposition of a 4-cm thick lead shield. According to the treatment group, a schedule delivering 0, 2.5, 5, or 7.5 Gy in a single fraction or 10.4 Gy in four consecutive fractions (2.6 Gy/day) was administered at a dose rate of 1.08 Gy/min. The 10.4 Gy dose represented the biologically equivalent dose of 7.5 Gy in a single fraction, as calculated using the linear quadratic model with an $\alpha/\beta = 10$.

Vaccination protocol

The STxB-E7 vaccine was produced by the chemical coupling of the N-bromoacetylated E7$_{43-57}$ peptide and the sulfhydryl group of a recombinant non-toxic Shiga toxin B-subunit variant, termed STxB/Cys, according to previously described procedures (22). Recombinant STxB/Cys was purified from bacterial periplasmic extracts as previously described (23). In brief, periplasmic extracts were loaded on a QHP column (GE Healthcare) and eluted in a linear NaCl gradient in Tris-HCl buffer. STxB/Cys containing fractions were pooled, validated for purity by SDSPAGE, and snap frozen in liquid nitrogen before storage at −80°C. The adjuvant α-galactosylceramide (KRN7000, Funakoshi, Japan) was administered alone or together with the first dose of vaccine. Vaccine and/or KRN7000 were administered i.p. at 20 and 1 μg per mouse, respectively.

CD8$^+$ T lymphocyte depletion

Mice received i.p. injections of 100 μg per mouse of anti-CD8 mAb (clone 2.43; BioXCell) or isotype control mAb on day 7 (one day before irradiation) to deplete CD8$^+$ T cells, as previously reported (20).

In vivo imaging

To monitor tumor growth, bioluminescence imaging was performed using the Xenogen *In Vivo* Imaging System 50 (IVIS; Caliper Life Sciences). Mice were placed in the supine position in the imaging chamber 5 minutes after i.p. injection of firefly luciferin; images were acquired whereas the mice were under sedation via the continuous administration of isoflurane. The photographic images and bioluminescence color images were superimposed, and signal quantification was performed using the LivingImage V 4.3.1 software (Caliper Life Sciences).

Tumor histopathology and vascular assessment

Immunohistochemistry for alpha smooth muscle actin (αSMA) was performed using a validated standard protocol on a Ventana Discovery Ultra autostainer (Roche Tissue Diagnostics; primary Ab ref ab5694, Abcam). Manual staining protocols on OCT frozen sections were used to detect CD31 (BD Pharmingen ref 553370), and ICAM-1 (Abcam ref ab25375). Slides were counterstained with hematoxylin. NG2 (primary Ab: Millipore ref AB5320) was detected by immunofluorescence. CD31 and αSMA staining were quantified using the algorithm for vessel detection in the Tissue Studio software package from Definiens

(Definiens). Vessels were automatically detected according to their IHC staining spectral properties in regions of interest that had been manually selected. The percentage of the area stained for NG2 was measured using the ImageJ v1.41 software. ICAM-1 staining was determined using a semiquantitative score based on the staining area (less than 1/field = 0; 1–2/field = 1; 3 or more/field = 2) and intensity (no staining = 0; weak = 1; moderate = 2; strong = 3).

Tumor vascular permeability by Miles assay

To assess vascular permeability, 0.2 mL Evans Blue dye (0.5%) was administered by tail vein injection. Mice were sacrificed 30 minutes after the injection. Dissected tumor samples were eluted in formaldehyde (0.5 mL for 50 mg of tissue) at 58°C overnight. The concentration of the accumulated dye for each aliquot was quantified by the use of a spectrophotometer by reading the absorbance at 620 nm with subtraction of the reference absorbance at 730 nm.

Analysis of tumor-infiltrating–specific CD8$^+$ T cells

To detect tumor infiltrating anti-E7$_{49-57}$/D^b–specific CD8$^+$ T cells, tumors were dissociated, washed twice in PBS and then incubated with the Fc receptor block CD16/CD32 (eBioscience). Tumors were then labeled with the E7$_{49-57}$/D^b tetramer according to the manufacturer's recommendations (Beckman Coulter Immunomics) and the anti-CD8 antibody. Cells were incubated for 35 minutes at 4°C with the PE-labeled tetramer. After incubation and washes, the cells were labeled using the live/dead cell viability assay (Life Technologies) and anti-CD8 (APC-Cy7; eBioscience), PD1 (FITC; eBioscience), CTLA4 (Brilliant Violet 421; Biolegend), and Tim3 (APC; eBioscience) mAbs for 20 minutes to phenotype the tetramer-positive CD8$^+$ T cells. Irrelevant tetramers recognizing an LCMV-derived peptide in the context of D^b molecules were used.

CD8$^+$ cells were detected by flow cytometry and expressed as the percentage of total living cells using the FlowJo (Tree Star) software.

Statistical analysis

Survival data were analyzed using the Kaplan–Meier and log-rank tests for survival distribution. The bioluminescent signal as a measure of tumor size, the immune infiltrate, and tumor perfusion levels were analyzed using an ANOVA analysis followed by the Tukey *post hoc* test for multiple comparisons. Correlations were assessed using the Pearson correlation test. Statistical analyses were performed using Prism Version 6 (GraphPad).

Results

The therapeutic efficacy of the STxB-E7 vaccine in an orthotopic head and neck tumor model is strongly enhanced by local irradiation

Our objective was to evaluate whether radiotherapy could enhance the therapeutic potential of the STxB-E7 systemic vaccination for the treatment of HNSCC. To test this hypothesis, we used an orthotopic model of HNSCC cancer by grafting HPV16 E7-expressing TC-1/Luc cells at a submucosal site of the inner lip in C57BL/6 mice. We designed a treatment protocol combining local tumor irradiation (IR) with i.p. administration of STxB-E7 vaccine associated with the mucosal adjuvant KRN7000 (Fig. 1A). KRN7000, either alone or in combination with radiotherapy, did

not impact on tumor growth (Supplementary Fig. S1A); therefore, all experiments were performed with KRN7000-treated mice as control groups. Bioluminescent *in vivo* imaging (Fig. 1B) showed that the mice developed fast-growing tumors (Fig. 1C) that resulted in the survival of control mice for 2 weeks after TC1/Luc cell injection (Fig. 1D). Treatment with a single dose of 7.5 Gy IR resulted in a limited tumor growth delay with no significant increase of survival (Fig. 1B–D). In line with our previous results (20), systemic immunization with STxB-E7 only partially improved tumor control, but its combination with local radiotherapy led to an effective antitumor response and 70% of the mice were still alive 70 days after the tumor engraftment (Fig. 1D, $P < 0.001$ vs. control, log-rank test). The tumor burden of mice treated with the combined therapy was significantly smaller compared with the single therapy (IR or STxB-E7)–treated mice (Fig. 1C, $P < 0.01$, one-way ANOVA). Most of the mice of the combination therapy group had complete tumor clearance that lasted until the end of the 90-day observation period (Fig. 1B). To obtain a therapeutic synergy between radiotherapy and immunization, a specific dose threshold had to be attained because irradiation doses lower than 7.5 Gy did not significantly affect tumor growth, even in combination with STxB-E7 (Supplementary Fig. S1B). Of note, when the equivalent dose of 7.5 Gy was given in fractions to mimic a clinically relevant therapeutic regimen, tumor control by the combination treatment was still effective (Fig. 1E). These data, obtained using a relevant model of HNSCC, indicate that an approach based on STxB-E7 systemic vaccination in combination with local radiotherapy represents a powerful therapeutic strategy.

High levels of tumor-infiltrating and splenic antigen-specific CD8$^+$ T cells are induced by combined irradiation and vaccination

We hypothesized that the potent antitumor effect observed in mice treated with the combination of STxB-E7 and local irradiation could be linked to an enhanced immune response in this group. We thus characterized the population of tumor-infiltrating lymphocytes in mice treated by the different regimens. We first focused on the CD8$^+$ T-cell population because these cells play a pivotal role in the tumor control of TC1 cells (24). The CD8$^+$ level was low in control tumors, and almost no E7-specific CD8$^+$ T cells were found in this group (Fig. 2A). Irradiation alone was not sufficient to induce a CD8$^+$ infiltrate, whereas vaccination upregulated the percentage of E7-specific CD8$^+$ T cells, as demonstrated by the E7-tetramer analysis. When irradiation was added to STxB-E7 immunization, the infiltration of CD8$^+$ T cells was significantly enhanced (Fig. 2A, left). Most of the CD8$^+$ T cells were antigen-specific, as the level of E7 tetramer–positive CD8$^+$ T lymphocytes reached a surprising 67% in this group (Fig. 2A, right). We also performed an analysis of the E7-specific CD8$^+$ infiltrate by identifying the CTLA4-, PD1-, and Tim3-positive subpopulations, but we found no significant differences among the treatment groups (Supplementary Fig. S2A–S2C). The induction of a specific CD8$^+$ T-cell response was not restricted to the tumor but was rather systemic. Indeed, when we analyzed the percentage of E7-specific CD8$^+$ T cells in the spleen, the combination of irradiation and vaccination resulted in the highest antigen-directed response compared with vaccine treatment alone (Fig. 2B). Moreover, the percentage of intratumoral E7-specific CD8$^+$ lymphocytes was inversely correlated with the tumor size (P
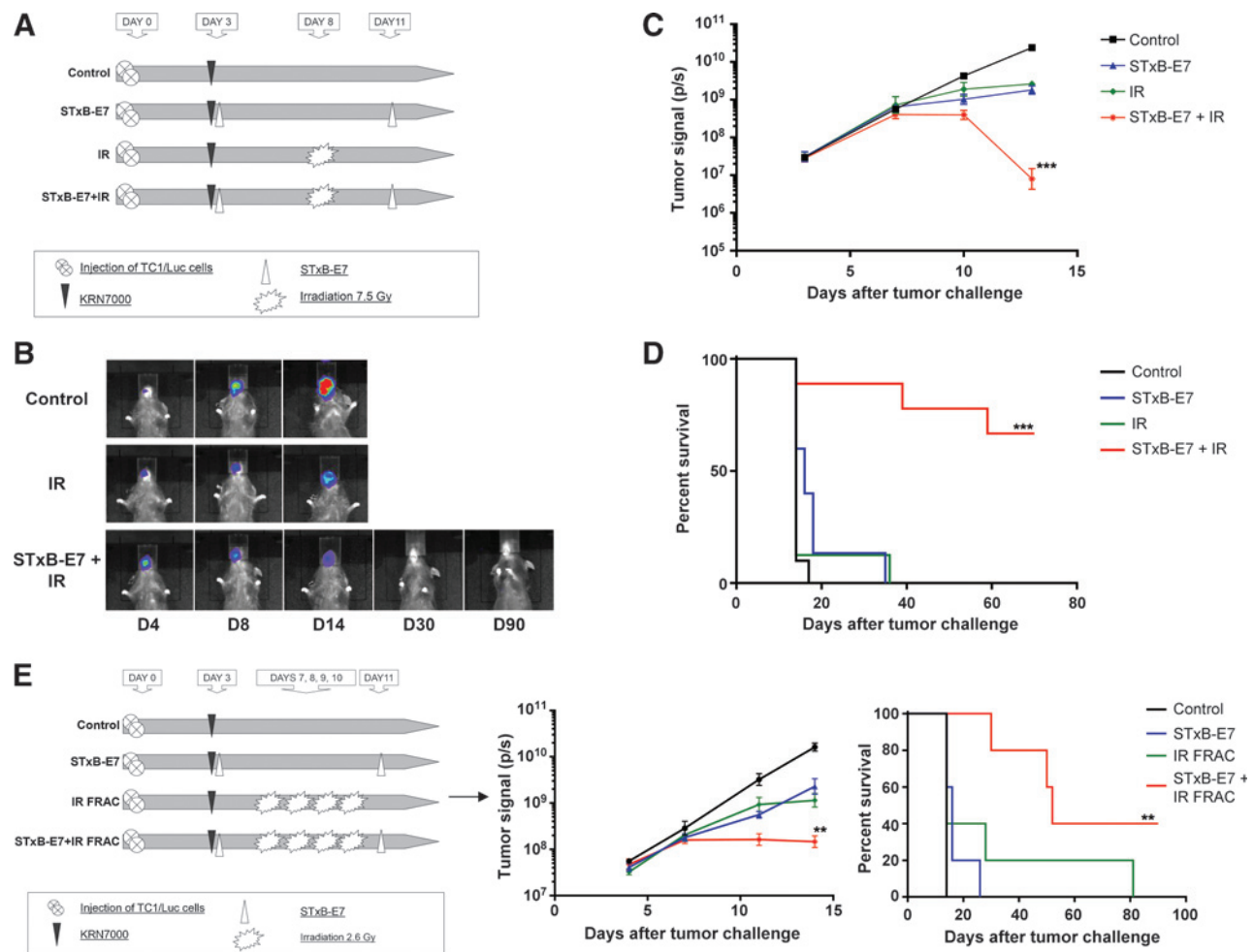
Figure 1.
Combination treatment by local radiation and therapeutic STxB-E7 vaccine elicits an effective antitumor response in an orthotopic head and neck cancer model. At day 0, C57BL/6 mice were injected with TC1/Luc cells in the inner lip. Mice were then subjected to the therapeutic treatments as depicted in the schematic diagram (A; single 7.5 Gy irradiation, 10 mice per group) and (E; left, fractionated irradiation four times 2.6 Gy, 5 mice/group). *In vivo* bioluminescent imaging was performed to follow tumor growth (B), and quantification of the bioluminescent signal was performed (C and E, center). **, $P < 0.01$; ***, $P < 0.001$, one-way ANOVA followed by the Tukey post-test of tumor sizes at day 14. Kaplan–Meier survival curves for single dose (D) or fractionated (E, right) irradiation experiments are shown. **, $P < 0.01$; ***, $P < 0.001$ versus the control group, the log-rank test. One of two representative experiments is shown.

< 0.05, Pearson's correlation test, Fig. 2C), suggesting a central role for CD8^{+} T lymphocytes in the antitumor response in our preclinical HNSCC tumor model. To mechanistically validate the role of CD8^{+} T cells in this therapeutic setting, we injected mice undergoing combined irradiation and vaccination with anti-CD8 antibodies to deplete the CD8^{+} T lymphocytes. The administration of anti-CD8 antibodies reversed the antitumor response, resulting in a complete loss of efficacy of the combined treatment on tumor size and survival, as all of the CD8^{+}-depleted mice had to be euthanized together with the controls (Fig. 2D). These data clearly indicate that CD8^{+} T lymphocytes are required to elicit the antitumor response triggered by the combination of irradiation and vaccination.

Effective combination therapy induces T-cell memory

Because most of the mice that received the combination of STxB-E7 and IR showed a complete remission of the tumor (Fig. 1B), we wondered whether the sustained CD8^{+} T-cell response

observed in this group resulted in the development of an effective T-cell memory. To test this hypothesis, 4 mice that were still tumor free 90 days after tumor grafting, as observed by *in vivo* imaging (Fig. 3A and B), were challenged again with TC1/Luc cells in the submucosa of the opposite inner lip. Four days after the second injection, bioluminescence imaging showed that all mice were correctly engrafted, with tumor cells localized on left inner lip (see representative Fig. 3A, D''4). Five days later (day 8, D''8), without any additional treatment, the luciferase activity was completely absent, indicating a spontaneous clearance of the tumor cells. In contrast, treatment-naïve mice used as positive controls displayed a tumor growth curve similar to those depicted in Fig. 1C (not shown). When mice were euthanized to collect the spleens (14 days after the second TC1/Luc challenge), the same results were observed (Fig. 3A, D''14). Cytofluorimetric analysis showed that rechallenged mice displayed high percentages of E7-specific CD8^{+} T cells at similar levels to those of mice at the end of the combined treatment (Fig. 3C), indicating that the spontaneous antitumor

Mondini et al.
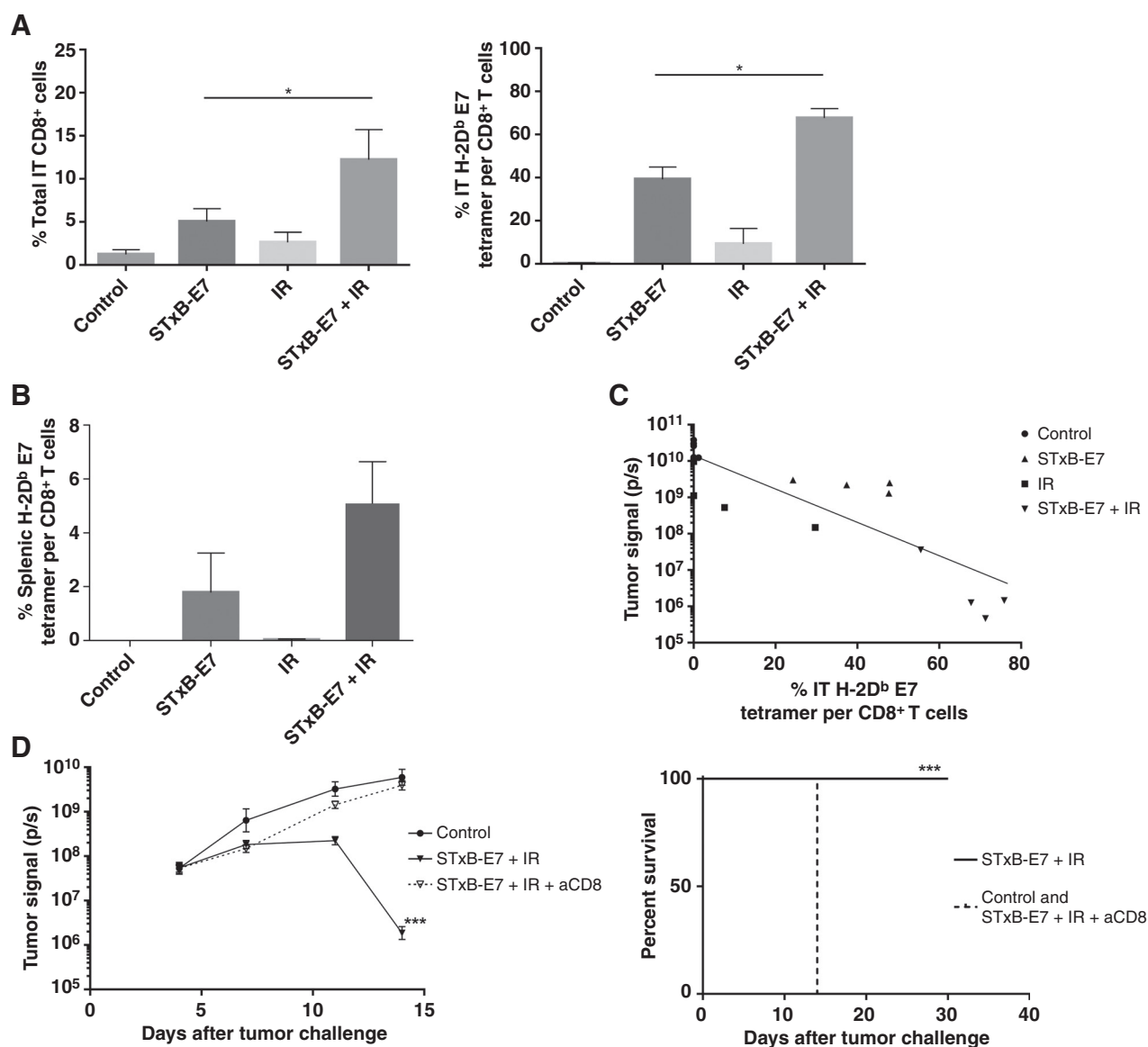
Figure 2.
A strong CD8^{+} T-cell response is elicited by combination treatment. Mice (5/group) were treated as described in Fig. 1 and tumor and spleen were collected at day 14. Intratumoral (IT) CD8^{+} T lymphocytes were detected by flow cytometry and expressed as the percentage of total living cells (A, left). E7-specific CD8^{+} T cells were detected by tetramer assay intratumorally (A, right) and in the spleen (B) and expressed as the mean ± SEM percentage of H-2Db E7$_{49-57}$-tetramer per CD8^{+} T cells; *, $P < 0.05$; one-way ANOVA followed by the Tukey post-test. C, tumor sizes obtained by IVIS *in vivo* imaging at the day of sacrifice are plotted against the percentage of tumor-infiltrating E7–specific CD8^{+}. Regression line is shown ($P < 0.05$, Pearson correlation test). D, anti-CD8 mAb or isotype control mAb were injected on day 7 (1 day before irradiation) to deplete CD8^{+} T cells. Mice (5/group) were then analyzed by *in vivo* bioluminescent imaging (left) and Kaplan–Meier survival curves were drawn (right); ***, $P < 0.001$, one-way ANOVA followed by the Tukey post-test of tumor sizes at day 14. One of two representative experiments is shown.

activity observed was linked to a persistent CD8^{+} response. A similar experiment was performed on three mice that were rechallenged with TC1/Luc cells 18 months after the first treatment, again resulting in the complete spontaneous rejection of tumor cells (not shown). It was also important to evaluate whether the immune response elicited from effective combined therapy provided protection against potential metastasis formation. We tested this by i.v. injecting TC1/Luc cells to induce the development of lung metastases. As shown by *in vivo* imaging analysis, in treatment-naïve mice, a bioluminescent signal localized to the lungs was already detectable four days after the

injection of TC1/Luc cells (Fig. 3D, left). The size of the lung metastases increased quickly until day 15, when the mice had to be euthanized. In mice that had already experienced a complete remission of the head and neck tumor upon administration of the combination of STxB-E7 and IR (rechallenge group), the tumor signal in the lungs was already smaller (or absent) at day 4 when compared with treatment-naïve mice. TC1/Luc cells were spontaneously cleared starting at day 8 (Fig. 3D, right) and all four tested mice remained metastasis-free until the end of the 60-day observation period (not shown). We repeated the same experiment by injecting TC1/Luc cells in 5 mice 9 months after the first
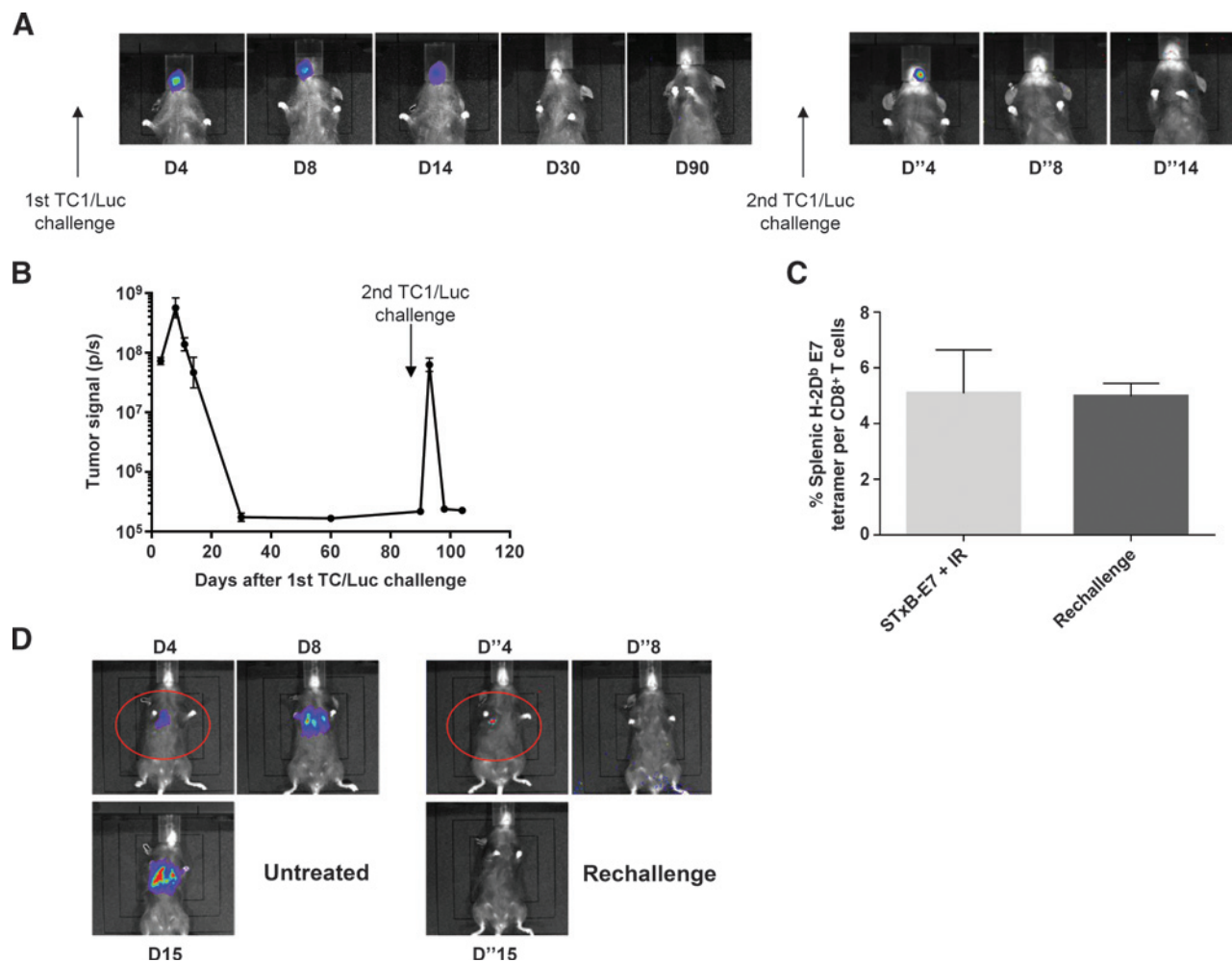
Figure 3.
Combination treatment induces a long-term antitumor immune response. Mice were treated with a combination of STxB-E7 vaccine and localized irradiation, as described in Fig. 1. Four mice that showed complete regression 3 months after the first TC1/Luc challenge were subjected to a second graft in the left inner lip. IVIS *in vivo* imaging was performed to follow tumor growth (A), and a quantification of the signal was performed (B). Mice were then euthanized 14 days after the second TC1/Luc challenge (D''14), and spleens were collected. C, splenic E7–specific CD8$^+$ T cells were detected using a tetramer assay (Rechallenge) and compared with those of mice that were subjected to combination treatment for the first time (STxB-E7+IR), as in Fig. 2B. D, IVIS *in vivo* imaging following i.v. injection of TC1/Luc in 4 treatment-naïve mice (left) and in 4 mice that showed complete regression 3 months after the first TC1/Luc challenge (right).

treatment, obtaining similar results (Supplementary Fig. S3). These data indicate that a combination of local irradiation and immunization elicits a CD8$^+$ T-cell memory that is sufficient to exert a complete antitumor response in both local recurrences and distant metastases.

Combined therapy promotes tumor vessel normalization

The increased efficacy of STxB-E7 vaccination observed upon irradiation can be at least partly linked to an increased accessibility of the tumor stroma by circulating leukocytes (25). We therefore analyzed the vascular structure in the different treatment groups. Immunohistochemical staining by the endothelial cell (EC) marker CD31 indicated that there were no significant differences in tumor vessel surface and density at either 24 hours (day 9) or 6 days after irradiation (day 14) that were elicited by the various treatments (Supplementary Fig. S4A and S4B). In contrast, when we analyzed the levels of pericytes by performing αSMA staining, we observed a significant increase in the stained surface in the

tumors of mice treated with both STxB-E7 and IR at day 14 (Fig. 4A). Because pericytes are recognized to be key regulators of the vascular structure and because the extent of their coverage on tumor vessels is typically diminished compared with normal tissues (26), these data suggest that the combined treatment induces a restoration of vascular functionality. This was further confirmed by the increase in NG2 staining (an alternative pericyte marker) observed at day 14 in mice treated with both local irradiation and vaccination (Fig. 4B and representative images in Supplementary Fig. S5A). These observations were supported by the Miles assay, a functional test that was performed to evaluate tumor vascular permeability (27). At 24 hours after irradiation (day 9), the permeability of tumor vessels was not yet affected by the treatments (Fig. 4C, left); however, at day 14 after tumor challenge, the permeability was significantly increased by the combined treatment compared with both control and single therapies (Fig. 4C, right). The observed increase was inversely correlated with the bioluminescent signal ($P < 0.05$, Pearson

Mondini et al.
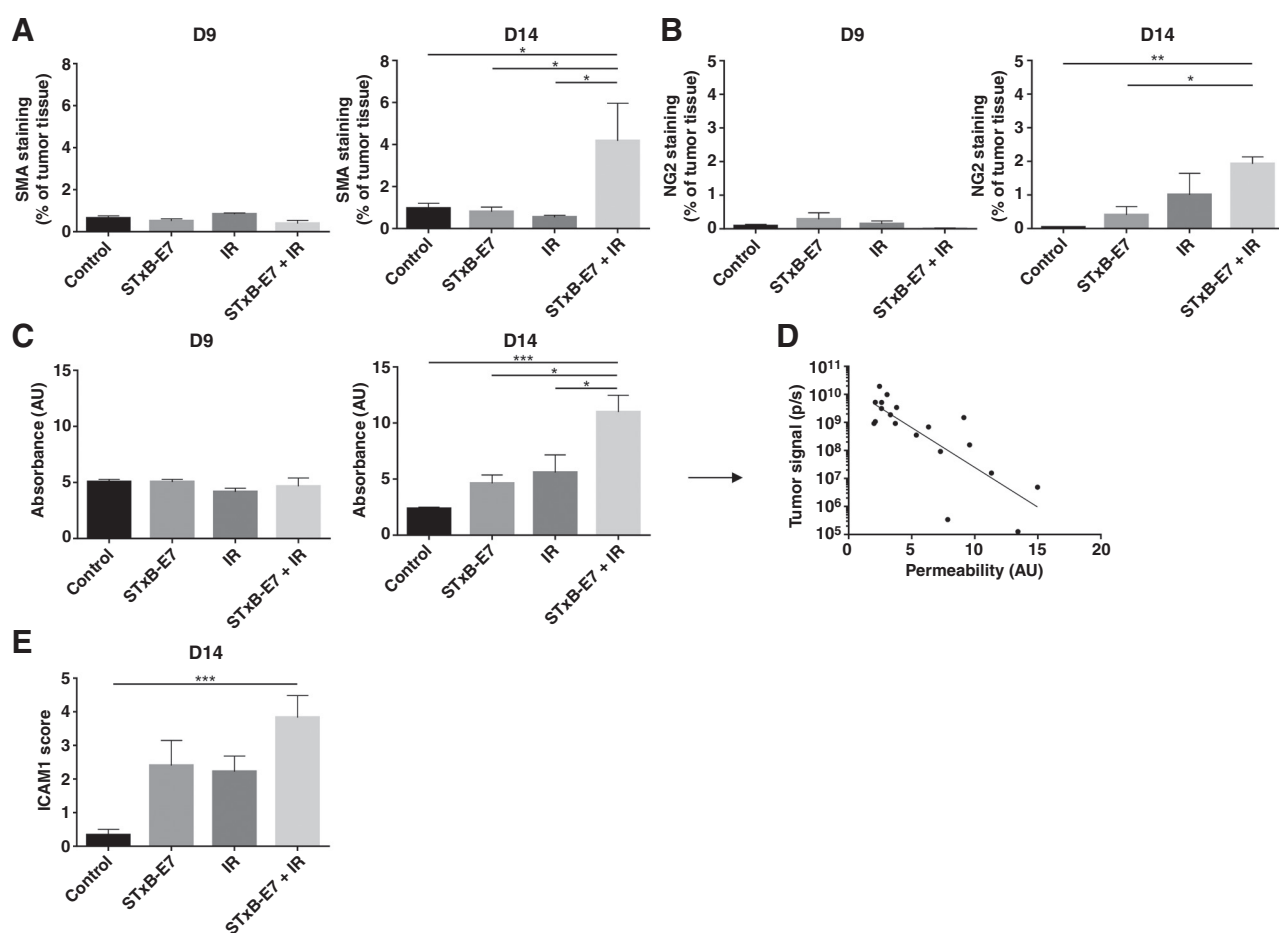
Figure 4.
Vascular normalization is induced by combination treatment. Mice were treated as described in Fig. 1 and tumors were collected at day 9 (D9) or 14 (D14). Staining by αSMA (A) or NG2 (B) antibody was performed, and quantification of the stained area is shown. C, mice received tail vein injections of 0.5% Evans Blue 30 minutes before sacrifice. Tumors were collected, and Evans Blue was eluted by O/N formamide incubation. The mean $\pm$ SEM absorbance corresponding to vascular permeability is depicted. D, data obtained by *in vivo* imaging at the day of sacrifice are plotted against absorbance at day 14 for individual mice to show the correlation between tumor vascular permeability and size. Regression line is shown ($P < 0.001$, Pearson correlation test). E, ICAM-1 expression was quantified on the basis of a score from immunohistochemical staining (see Materials and Methods); *, $P < 0.05$; **, $P < 0.01$; ***, $P < 0.001$ one-way ANOVA followed by the Tukey post-test.

correlation test, Fig. 4D), indicating that vascular permeability was linked to the tumor size at this time point. Finally, we evaluated vessel activation by detecting ICAM-1 expression in the tumors. ICAM-1, a transmembrane protein implied in the arrest and transmigration of leukocytes from blood vessels (28), was increased in tumors from mice undergoing the different treatments when compared with control mice; the highest score was observed in the combination group (Fig. 4E and representative images in Supplementary Fig. S5B). Taken together, these data indicate that the combination of STxB-E7 immunization and irradiation promotes tumor vessel normalization, which can favor the recruitment and infiltration of leukocytes in the tumor tissue.

Discussion

There is currently a growing interest in combination approaches based on radiotherapy and immunotherapy for the treatment of solid tumors, and cancer vaccines could play an important role in this setting (12). Peptide vaccines coupled to the

non-toxic STxB have been successfully tested in several preclinical settings and represent a promising tool for vaccine-based cancer therapy (20, 29–31). Nevertheless, their use in association with radiotherapy has not been previously reported. Here, we report a novel, extremely effective combination of STxB-based vaccination (STxB-E7 vaccine) and local irradiation for the treatment of HPV-associated HNSCC. In our murine model, this novel therapeutic approach resulted in the complete clearance of the majority of treated tumors. The new STxB-based vaccination strategy acted synergistically with either single dose or fractionated irradiation, which is of particular relevance because fractionated radiotherapy is a mainstay for the treatment of HNSCC (32).

In agreement with previous observations (11, 20), the antitumor response in our preclinical model was dependent on CD8^{+} T-cell activity (Fig. 2D). Previously, we have shown that the homing of T cells to mucosal tumors is improved by intranasal immunization (20). Here, we demonstrate that irradiation overcomes the necessity of intranasal (mucosal) immunization with STxB-E7, because high levels of tumor-infiltrating, antigen-specific CD8^{+} T lymphocytes are obtained after i.p. administration (Fig. 2A and

2B). The high number of CD8$^+$ T cells observed upon combined treatment was required to trigger the potent antitumor response, since the low CD8$^+$ levels detected upon systemic vaccination alone were not sufficient to induce tumor control and regression (Fig. 1B). Our data, thus, suggest that a threshold level of antigen-specific CD8$^+$ lymphocytes should be reached to overtake the tumor growth, resulting in tumor clearance, and that irradiation enhances the vaccine-induced CD8$^+$ response above this required level.

Combined therapy can promote the infiltration by leukocytes by affecting the tumor stroma, specifically the vessels. Vascular normalization has been proposed to be a key mechanism in mediating antitumor responses (33, 34), enhancing cancer immunotherapy (16, 35). Moreover, endothelial cells within tumors often display a downregulation of ICAM-1/2, VCAM-1, and CD34, a phenomenon defined as "EC anergy" (36). Restoration of the expression of such adhesion molecules can facilitate the interaction of effector T cells with ECs, promoting their migration through blood vessels. Here, we show for the first time that a combination therapy based on irradiation and vaccination induces increased tumor vascular permeability (Fig. 4C), which is accompanied by augmented pericyte coverage (Fig. 4A and 4B) and ICAM-1 expression (Fig. 4D). We also observed a threshold dose for synergy between irradiation and vaccine in the range of 7.5 Gy. Accordingly, it has been shown that vascular-induced changes occur in a dose-dependent manner after a single dose of irradiation (37). In their recent work, Klug and colleagues (38) reported a reduction in vessels area and density (which we did not observe) in a pancreatic carcinoma model upon low-dose irradiation and T-cell transfer. They also observed a macrophage repolarization toward M1, whereas our preliminary results did not suggest this repolarization (data not shown), thus highlighting the specificities of different tumor settings. In addition, in contrast with other studies (11, 39), the combination of irradiation and the cancer vaccine used here did not result in an increase in immunosuppressive cells in the tumor microenvironment (data not shown). The use of a mucosal tumor model and some specific features of each vaccine may explain these differences.

In addition to vascular effects, the synergy between IR and STxB-E7 could be also linked to the induction of immunologic cell death by radiotherapy. Immunologic cell death, when dying cells display immunologically favorable features, has indeed been suggested as a major mechanism of synergy between immunomodulation and irradiation (40). Because STxB-E7 directly targets DCs, another potential mechanism of interplay between irradiation and vaccination could be through the modulation of the function of DCs by ionizing radiation, as reported in *in vitro* settings (41). Experimental work is currently ongoing to elucidate these mechanisms.

Recently, two vaccines targeting HPV antigens have been tested in association with radiotherapy in murine models (11, 39). However, though HPV-associated cancers are located in mucosal sites, both studies were conducted using subcutaneous tumors. Our recent data indicate that the site of tumor implantation affects the response to cancer vaccine and the homing of induced CD8$^+$ cells (20). It was, therefore, important to test the efficacy of irradiation combined with vaccination in a model more closely reproducing the natural lesions in humans, such as the mucosal murine model of HNSCC used here. Moreover, we were able to demonstrate the powerful antitumor efficacy of the combination treatment at much lower irradiation doses (7.5 Gy compared with

the dose of 14 Gy used in the previous studies). Radiotherapy dose reduction can limit the risk of late complications, and is a lively area of investigation (42). The possibility to use low irradiation doses could be a valuable tool for treatment deintensification strategies in the clinic. Wu and colleagues (11), Draghiciu and colleagues (39) performed radiotherapy before vaccination, whereas we administered STxB-E7 before irradiation. This approach might facilitate the implementation of vaccinations in future clinical strategies because patients with a confirmed diagnosis of HPV-positive HNSCC would immediately benefit from the vaccination administration while waiting for radiotherapy treatment.

The combination of local irradiation and immunotherapy has recently been presented as a means to exert better local tumor control; however, in specific settings, it also triggers a systemic antitumor effect, the so-called "abscopal" effect (43). In our study, when the combination treatment resulted in complete tumor clearance, which occurred in 70% of treated mice, no recurrence or metastasis was found, even after an 18-month observation period. This is a consequence of the induction of an effective T-cell memory, with a protective effect both locally and systemically, as demonstrated by our rechallenge experiments (Fig. 3 and Supplementary Fig. S3). This represents a promising clinical tool, because a patient treated with this combination therapy who undergoes tumor remission will likely be protected against any local or distant relapse.

There is a need for specific therapies to manage HPV-related tumors because HPV status is a biomarker of outcome and response to radiotherapy. Currently, there are no specific therapies that increase the therapeutic ratio for these tumors. The radio-vaccination strategy proposed here is a promising approach that can likely be transferred into early-phase clinical trials.

Disclosure of Potential Conflicts of Interest

No potential conflicts of interest were disclosed.

Authors' Contributions

Conception and design: M. Mondini, M.-C. Vozenin, J.-L. Perfettini, E. Tartour, E. Deutsch
Development of methodology: M. Mondini, M. Nizard, M. Loi, C. Clémenson, J. Adam, L. Johannes, E. Deutsch
Acquisition of data (provided animals, acquired and managed patients, provided facilities, etc.): M. Mondini, M. Nizard, T. Tran, L. Mauge, M. Loi, C. Clémenson, D. Dugue, P. Maroun, J. Adam, C. Badoual, E. Tartour
Analysis and interpretation of data (e.g., statistical analysis, biostatistics, computational analysis): M. Mondini, M. Nizard, T. Tran, L. Mauge, M. Loi, E. Louvet, D. Helley, E. Tartour
Writing, review, and/or revision of the manuscript: M. Mondini, M. Nizard, L. Mauge, M. Loi, C. Clémenson, P. Maroun, C. Badoual, D. Helley, L. Johannes, M.-C. Vozenin, J.-L. Perfettini, E. Tartour, E. Deutsch
Administrative, technical, or material support (i.e., reporting or organizing data, constructing databases): M. Mondini, M. Loi, D. Dugue, E. Dransart
Study supervision: M. Mondini, E. Deutsch

Acknowledgments

References

1. De Vuyst H, Clifford G, Li N, Franceschi S. HPV infection in Europe. Eur J Cancer 2009;45:2632–9.
2. Satterwhite CL, Torrone E, Meites E, Dunne EF, Mahajan R, Ocfemia MC, et al. Sexually transmitted infections among US women and men: prevalence and incidence estimates, 2008. Sex Transm Dis 2013; 40:187–93.
3. Arbyn M, de Sanjose S, Saraiya M, Sideri M, Palefsky J, Lacey C, et al. EUROGIN 2011 roadmap on prevention and treatment of HPV-related disease. Int J Cancer 2012;131:1969–82.
4. Zaravinos A. An updated overview of HPV-associated head and neck carcinomas. Oncotarget 2014;5:3956–69.
5. Weinberger PM, Yu Z, Haffty BG, Kowalski D, Harigopal M, Brandsma J, et al. Molecular classification identifies a subset of human papillomavirus–associated oropharyngeal cancers with favorable prognosis. J Clin Oncol 2006;24:736–47.
6. Ang KK, Sturgis EM. Human papillomavirus as a marker of the natural history and response to therapy of head and neck squamous cell carcinoma. Semin Radiat Oncol 2012;22:128–42.
7. Lassen P. The role of Human papillomavirus in head and neck cancer and the impact on radiotherapy outcome. Radiother Oncol 2010; 95:371–80.
8. Kantoff PW, Higano CS, Shore ND, Berger ER, Small EJ, Penson DF, et al. Sipuleucel-T immunotherapy for castration-resistant prostate cancer. N Engl J Med 2010;363:411–22.
9. Klebanoff CA, Acquavella N, Yu Z, Restifo NP. Therapeutic cancer vaccines: are we there yet? Immunol Rev 2011;239:27–44.
10. Harris TJ, Hipkiss EL, Borzillary S, Wada S, Grosso JF, Yen HR, et al. Radiotherapy augments the immune response to prostate cancer in a time-dependent manner. Prostate 2008;68:1319–29.
11. Wu CY, Yang LH, Yang HY, Knoff J, Peng S, Lin YH, et al. Enhanced cancer radiotherapy through immunosuppressive stromal cell destruction in tumors. Clin Cancer Res 2014;20:644–57.
12. Formenti SC, Demaria S. Combining radiotherapy and cancer immunotherapy: a paradigm shift. J Natl Cancer Inst 2013;105:256–65.
13. Levy A, Chargari C, Cheminant M, Simon N, Bourgier C, Deutsch E. Radiation therapy and immunotherapy: implications for a combined cancer treatment. Crit Rev Oncol Hematol 2013;85:278–87.
14. Schaue D, Ratikan JA, Iwamoto KS, McBride WH. Maximizing tumor immunity with fractionated radiation. Int J Radiat Oncol Biol Phys 2012;83:1306–10.
15. Welters MJ, Kenter GG, Piersma SJ, Vloon AP, Lowik MJ, Berends-van der Meer DM, et al. Induction of tumor-specific CD4$^+$ and CD8$^+$ T-cell immunity in cervical cancer patients by a human papillomavirus type 16 E6 and E7 long peptides vaccine. Clin Cancer Res 2008;14:178–87.
16. Huang Y, Goel S, Duda DG, Fukumura D, Jain RK. Vascular normalization as an emerging strategy to enhance cancer immunotherapy. Cancer Res 2013;73:2943–8.
17. Vingert B, Adotevi O, Patin D, Jung S, Shrikant P, Freyburger L, et al. The Shiga toxin B-subunit targets antigen *in vivo* to dendritic cells and elicits anti-tumor immunity. Eur J Immunol 2006;36:1124–35.
18. Adotevi O, Vingert B, Freyburger L, Shrikant P, Lone YC, Quintin-Colonna F, et al. B subunit of Shiga toxin-based vaccines synergize with alpha-galactosylceramide to break tolerance against self antigen and elicit anti-viral immunity. J Immunol 2007;179:3371–9.
19. Bishop JA, Ma XJ, Wang H, Luo Y, Illei PB, Begum S, et al. Detection of transcriptionally active high-risk HPV in patients with head and neck squamous cell carcinoma as visualized by a novel E6/E7 mRNA in situ hybridization method. Am J Surg Pathol 2012; 36:1874–82.
20. Sandoval F, Terme M, Nizard M, Badoual C, Bureau MF, Freyburger L, et al. Mucosal imprinting of vaccine-induced CD8(+) T cells is crucial to inhibit the growth of mucosal tumors. Sci Transl Med 2013;5: 172ra20.
21. Fumagalli I, Dugue D, Bibault JE, Clemenson C, Vozenin MC, Mondini M, et al. Cytotoxic effect of lapatinib is restricted to human papillomavirus-positive head and neck squamous cell carcinoma cell lines. Onco Targets Ther 2015;8:335–45.
22. Haicheur N, Bismuth E, Bosset S, Adotevi O, Warnier G, Lacabanne V, et al. The B subunit of Shiga toxin fused to a tumor antigen elicits CTL and targets dendritic cells to allow MHC class I-restricted presentation of peptides derived from exogenous antigens. J Immunol 2000;165: 3301–8.
23. Mallard F, Johannes L. Shiga toxin B-subunit as a tool to study retrograde transport. Methods Mol Med 2003;73:209–20.
24. Badoual C, Hans S, Merillon N, Van Ryswick C, Ravel P, Benhamouda N, et al. PD-1-expressing tumor-infiltrating T cells are a favorable prognostic biomarker in HPV-associated head and neck cancer. Cancer Res 2013;73:128–38.
25. Johansson A, Ganss R. Remodeling of tumor stroma and response to therapy. Cancers (Basel) 2012;4:340–53.
26. Armulik A, Genove G, Betsholtz C. Pericytes: developmental, physiological, and pathological perspectives, problems, and promises. Dev Cell 2011;21:193–215.
27. Ibla JC, Khoury J. Methods to assess tissue permeability. Methods Mol Biol 2013;1066:81–8.
28. Lawson C, Wolf S. ICAM-1 signaling in endothelial cells. Pharmacol Rep 2009;61:22–32.
29. Haicheur N, Benchetrit F, Amessou M, Leclerc C, Falguieres T, Fayolle C, et al. The B subunit of Shiga toxin coupled to full-size antigenic protein elicits humoral and cell-mediated immune responses associated with a Th1-dominant polarization. Int Immunol 2003;15:1161–71.
30. Maak M, Nitsche U, Keller L, Wolf P, Sarr M, Thiebaud M, et al. Tumor-specific targeting of pancreatic cancer with Shiga toxin B-subunit. Mol Cancer Ther 2011;10:1918–28.
31. Sadraeian M, Khoshnood Mansoorkhani MJ, Mohkam M, Rasoul-Amini S, Hesaraki M, Ghasemi Y. Prevention and inhibition of TC-1 cell growth in tumor bearing mice with HPV16 E7 protein in fusion with Shiga toxin B-subunit from shigella dysenteriae. Cell J 2013;15:176–81.
32. Argiris A, Karamouzis MV, Raben D, Ferris RL. Head and neck cancer. Lancet 2008;371:1695–709.
33. Goel S, Wong AH, Jain RK. Vascular normalization as a therapeutic strategy for malignant and nonmalignant disease. Cold Spring Harb Perspect Med 2012;2:a006486.
34. Heath VL, Bicknell R. Anticancer strategies involving the vasculature. Nat Rev Clin Oncol 2009;6:395–404.
35. Demaria S, Pilones KA, Vanpouille-Box C, Golden EB, Formenti SC. The optimal partnership of radiation and immunotherapy: from preclinical studies to clinical translation. Radiat Res 2014;182:170–81.
36. Bellone M, Calcinotto A. Ways to enhance lymphocyte trafficking into tumors and fitness of tumor infiltrating lymphocytes. Front Oncol 2013;3:231.
37. Garcia-Barros M, Paris F, Cordon-Cardo C, Lyden D, Rafii S, Haimovitz-Friedman A, et al. Tumor response to radiotherapy regulated by endothelial cell apoptosis. Science 2003;300:1155–9.

38. Klug F, Prakash H, Huber PE, Seibel T, Bender N, Halama N, et al. Low-dose irradiation programs macrophage differentiation to an iNOS(+)/M1 phenotype that orchestrates effective T cell immunotherapy. Cancer Cell 2013;24:589–602.

39. Draghiciu O, Walczak M, Hoogeboom BN, Franken KL, Melief KJ, Nijman HW, et al. Therapeutic immunization and local low-dose tumor irradiation, a reinforcing combination. Int J Cancer 2014;134:859–72.

40. Galluzzi L, Kepp O, Kroemer G. Immunogenic cell death in radiation therapy. Oncoimmunology 2013;2:e26536.

41. Jahns J, Anderegg U, Saalbach A, Rosin B, Patties I, Glasow A, et al. Influence of low dose irradiation on differentiation, maturation and T-cell activation of human dendritic cells. Mutat Res 2011;709–710:32–9.

42. Quon H, Richmon JD. Treatment deintensification strategies for HPV-associated head and neck carcinomas. Otolaryngol Clin North Am 2012;45:845–61.

43. Tang C, Wang X, Soh H, Seyedin S, Cortez MA, Krishnan S, et al. Combining radiation and immunotherapy: a new systemic therapy for solid tumors? Cancer Immunol Res 2014;2:831–8.

Molecular Cancer Therapeutics

Synergy of Radiotherapy and a Cancer Vaccine for the Treatment of HPV-Associated Head and Neck Cancer

Michele Mondini, Mevyn Nizard, Thi Tran, et al.

Updated version	Access the most recent version of this article at: doi:10.1158/1535-7163.MCT-14-1015
Supplementary Material	Access the most recent supplemental material at: http://mct.aacrjournals.org/content/suppl/2015/04/01/1535-7163.MCT-14-1015.DC1

Cited articles	This article cites 42 articles, 12 of which you can access for free at: http://mct.aacrjournals.org/content/14/6/1336.full#ref-list-1
Citing articles	This article has been cited by 3 HighWire-hosted articles. Access the articles at: http://mct.aacrjournals.org/content/14/6/1336.full#related-urls

E-mail alerts	Sign up to receive free email-alerts related to this article or journal.
Reprints and Subscriptions	To order reprints of this article or to subscribe to the journal, contact the AACR Publications Department at pubs@aacr.org.
Permissions	To request permission to re-use all or part of this article, use this link http://mct.aacrjournals.org/content/14/6/1336. Click on "Request Permissions" which will take you to the Copyright Clearance Center's (CCC) Rightslink site.